






Cite this: *Chem. Sci.*, 2024, 15, 12543

All publication charges for this article have been paid for by the Royal Society of Chemistry

Development of non-closed silver clusters by transition-metal-coordination-cluster substituted polyoxometalate templates†

Rui Ge, Ping-Wei Cai,  Cai Sun,  Yan-Qiong Sun,  Xin-Xiong Li * and Shou-Tian Zheng *

Nature seems to favor the formation of closed anion-templated silver clusters. How precisely to create non-closed silver clusters remains an interesting challenge. In this work, we propose that the use of transition-metal-coordination-cluster substituted polyoxometalates (TMCC-substituted POMs) as templates is an effective synthetic strategy for creating the non-closed silver clusters, as demonstrated by the obtainment of four types of rare non-closed silver cluster species of $\text{Ag}_{38}\text{-TM}$ (TM = Co, Ni or Zn), $\text{Ag}_{37}\text{-Zn}$, $\{\text{Ag}_{37}\text{-Zn}\}_\infty$ and $\text{Ag}_{36}\text{-TM}$ (TM = Co, Ni). The idea of the strategy is to employ the TMCC-substituted POMs containing cluster modules with different bond interactions with Ag^+ ions as templates to guide the formation of the non-closed silver clusters. For example, TMCC-substituted POM clusters are used as templates in this work, which contain POM modules that can coordinate with the Ag^+ ions and TMCC moieties that are difficult to coordinate with the Ag^+ ions, leading to the Ag^+ ions being unable to form closed clusters around TMCC-substituted POM templates. The work demonstrates a promising approach to developing intriguing and unexplored non-closed silver clusters.

Received 4th March 2024
Accepted 22nd June 2024

DOI: 10.1039/d4sc01502a

rsc.li/chemical-science

Introduction

The pursuit of crystalline silver clusters has progressed rapidly in the past two decades because such materials not only have fascinating structures but also exhibit promising properties in sensing, energy storage, optoelectronics, and catalysis.^{1–7} In this area, anions have been widely used as structure-directing agents to induce the formation of new high-nuclearity silver clusters,^{8–10} and they perform multiple roles in determining the structures and properties of the silver clusters. They can serve as anionic templates to organize the Ag^+ ions together in an ordered way, control the nuclearity, size, and shape of the silver clusters, stabilize the silver clusters by balancing positive charges and electronic communications, and transfer functions into final silver clusters.^{11,12} Given these advantages, various inorganic anions have been introduced to template the organization of the Ag^+ ions, leading to the rapid development of the anion-templated silver clusters in recent years.^{13–15}

Nevertheless, the vast majority of known anion-templated silver clusters possess closed structures, while the non-closed

silver clusters have rarely been reported.^{16–19} Compared with closed silver clusters, non-closed ones are more appealing and favorable, as they may provide atomic-level information on the formation of the closed silver clusters and possess exposed active sites that may endow them with unique physicochemical properties.¹⁸ However, the efficient fabrication of the non-closed silver clusters still remains a challenging task, and a controllable synthetic method has yet to be developed.

Due to the uniform distribution of negative charges and coordination sites of commonly used inorganic anions or anion clusters, the Ag^+ ions tend to spontaneously form closed cluster structures around these anion templates.^{20,21} As shown in Fig. 1, will it be possible to prevent the Ag^+ ions from forming closed structures? Are there any feasible strategies capable of effectively creating the non-closed silver clusters? Given that the synthetic chemistry of the silver clusters has been of wide



Fig. 1 Structure and synthesis of the closed and non-closed silver clusters.

Fujian Provincial Key Laboratory of Advanced Inorganic Oxygenated Materials, College of Chemistry, Fuzhou University, Fuzhou 350108, Fujian, China. E-mail: lxz@fzu.edu.cn; stzheng@fzu.edu.cn

† Electronic supplementary information (ESI) available: The Supporting Information contains a complete general experimental section, including all procedures and equipment used. CCDC 2154076, 2261863, 2261850, 2154079, 2261845, 2269039, and 2154081. For ESI and crystallographic data in CIF or other electronic format see DOI: <https://doi.org/10.1039/d4sc01502a>

interest,^{22–25} it is of significant scientific interest to investigate the possibility of the construction of the non-closed silver clusters.

Polyoxometalates (POMs) are a class of early-transition-metal–oxygen clusters assembled from corner-, edge-, or face-sharing MO_n (M generally refers to V, Mo, W, Nb, or Ta) polyhedra with M in high oxidation states. Due to their attractive structural characteristics (nanosize, high negative charge, and redox) and wide potential applications in catalysis, electronics, and biomedicine,^{26–32} POMs have been explored as the anionic templates for the construction of high nuclear silver clusters. However, as with commonly used anionic templates, POMs have uniformly distributed negative charges and coordination sites that usually induce the Ag^+ ions to form the closed clusters.

One area of particular interest is that POMs can lose one or more MO_n polyhedra *via* hydrolytic degradation to generate various lacunary POMs, which allows the introduction of transition-metal-coordination-clusters (TMCCs) into their vacancies to form intriguing and diverse TMCC-substituted POMs. The use of the TMCC-substituted POM clusters with different cluster modules (TMCCs and POMs) within same molecules as the templates would be highly desirable for the development of intriguing and rare non-closed silver clusters because the POM modules can template the formation of the silver clusters by the formation of coordination bonds between terminal oxygen and the Ag^+ ions, while terminal ligands on the TMCC module can prevent TMCC from bonding to the Ag^+ ions. Thus, the combination of POM and TMCC endows the TMCC-substituted POM templates with regions that show distinct bonding interactions with the Ag^+ ions, which can make the Ag^+ ions form the non-closed silver clusters around the whole TMCC-substituted POM cluster template.

Here, for the first time, we report the introduction of the TMCC-substituted POMs into the silver clusters and successful obtainment of a family of the rare non-closed silver cluster species of $\{[\text{TM}_4(\mu_3\text{-OH})_3(\text{Ac})_3\text{SiW}_9\text{O}_{34}]\text{Ag}_{38}(\text{BuC}\equiv\text{C})_{21}(\text{NO}_3)_4\text{CH}_3\text{CN}\}(\text{Ac})_5$ (**Ag₃₈-TM**) (TM = Zn/Ni/Co; $\text{Bu} =$ tertiary butyl; $\text{Ac}^- = \text{CH}_3\text{COO}^-$), $\{[\text{Zn}_5(\mu_3\text{-OH})_3(\text{Ac})_2(\text{SiW}_9\text{O}_{34})(\text{SiW}_{11}\text{O}_{39})]\text{Ag}_{37}(\text{BuC}\equiv\text{C})_{22}(\text{NO}_3)(\text{CH}_3\text{CN})_2(\text{NO}_3)\cdot(\text{CH}_3\text{CN})_2$ (**Ag₃₇-Zn**), $\text{Ag}_{0.65}\{[\text{Zn}_5(\mu_3\text{-OH})_3(\text{Ac})_2(\text{SiW}_9\text{O}_{34})(\text{SiW}_{11}\text{O}_{39})]\text{Ag}_{37}(\text{BuC}\equiv\text{C})_{19}(\text{NO}_3)_2\}_2(\text{Ac})_{6.65}$ (**Ag₃₇-Zn**) $_{\infty}$ and $\{[\text{TM}_5(\mu_3\text{-OH})_3(\text{Ac})_2(\text{SiW}_9\text{O}_{34})(\text{SiW}_{11}\text{O}_{39})]\text{Ag}_{36}(\text{BuC}\equiv\text{C})_x(\text{Ac})_{23-x}2\text{CH}_3\text{CN}$ (**Ag₃₆-TM**) (TM = Co/Ni; $x = 18/17$ for Co/Ni), which demonstrate that the use of the TMCC-substituted POMs as the templates is an effective synthetic strategy for the creation of the non-closed silver clusters.

Results and discussion

The crystals of the four types of compounds were obtained by solvothermal reactions of $\text{AgNO}_3/\text{CF}_3\text{SO}_3\text{Ag}$, $\text{BuC}\equiv\text{CAg}$, $(\text{Bu}_4\text{-N})_6\text{H}_4[\text{SiW}_9\text{O}_{34}]$ and $\text{TM}(\text{Ac})_2\cdot x\text{H}_2\text{O}$ in CH_3CN (see the experimental details in ESI, Fig. S1†). Given the isomorphism, only **Ag₃₈-Zn** is chosen as a representative of **Ag₃₈-TM** for single-crystal X-ray diffraction (SCXRD) analysis description. **Ag₃₈-Zn** crystallizes in the triclinic $\bar{P}1$ space group and comprises a zinc-cluster-substituted POM core of $\{[\text{Zn}_4(\mu_3\text{-OH})_3(\text{Ac})_3\text{SiW}_9\text{O}_{34}]\}$

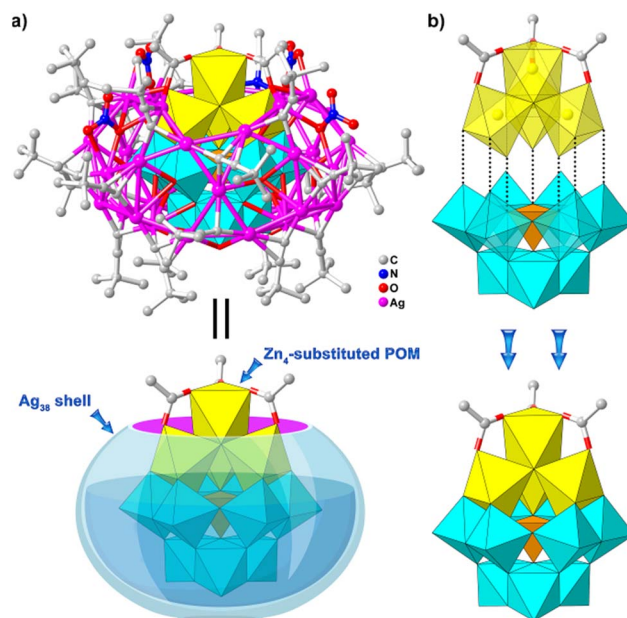


Fig. 2 (a) and (b) View of the structures of **Ag₃₈-Zn** and the **Zn₄SiW₉** template, respectively. Polyhedral code: WO_6 , cyan; SiO_4 , orange; and ZnO_6 , yellow (the same thereafter).

(**Zn₄SiW₉**) surrounded by a unique 38-nuclearity non-closed silver shell of $\{\text{Ag}_{38}(\text{BuC}\equiv\text{C})_{21}(\text{NO}_3)_4\text{CH}_3\text{CN}\}$ (**Ag₃₈**) (Fig. 2a). The inner **Zn₄SiW₉** template can be described as a tetra-nuclear $\{\text{Zn}_4(\mu_3\text{-OH})_3(\text{Ac})_3\}$ (**Zn₄**) zinc coordination cluster trapped into vacant sites by a trilacunary Keggin-type $\{\text{SiW}_9\text{O}_{34}\}$ POM through the sharing of nine oxygen atoms (Fig. 2b). **Zn₄** consists of four edge-sharing octahedral-coordinated Zn^{2+} ions integrated by three $\mu_3\text{-OH}$ groups, three of which are exactly located on the vacant sites of trilacunary POM to give a triangular $\{\text{Zn}_3(\mu_3\text{-OH})_3\}$ trimer, and the fourth Zn^{2+} ion is capped onto the planar trimer by sharing three $\mu_3\text{-OH}$ groups and three terminal acetate ligands.

Interestingly, the presence of the terminal acetate ligands prevents the possibility of coordination between zinc clusters and the Ag^+ ions. As a result, the **Zn₄SiW₉** template allows the formation of a non-closed nest-shaped **Ag₃₈** shell through Ag–O bonds ranging from 2.381 to 2.597 Å (Fig. 2a). As shown in Fig. S2†, Ag^+ atoms are arranged into a sandwich-type three-layer structure protected by 21 $\text{BuC}\equiv\text{C}^-$ ligands, 4 NO_3^- and 1 terminal CH_3CN molecule. Upper and basal layers can be described as a larger **Ag₁₁** ring and small **Ag₉** ring, and upper and lower rings are interlinked by three silver ions and three **Ag₅** tetragonal pyramids in an alternating arrangement, leading to the overall **Ag₃₈** shell with Ag–Ag distances in the range of 2.849 to 3.965 Å. $\text{BuC}\equiv\text{C}^-$ and CH_3CN ligands adopt a μ_3 -bridging mode to cap the **Ag₃₈** shell (Fig. S2†), each of which is ligated to three Ag^+ ions (Ag–C: 1.919–2.409 Å; Ag–N: 2.104–2.269 Å). Half of the 4 NO_3^- anions are situated on the top of the **Ag₁₁** ring *via* a $\mu_3\text{-}\eta_2\text{-}\eta_1$ coordination mode, and the remaining two NO_3^- anions connect the **Ag₁₁** ring with two **Ag₅** tetragonal pyramids, respectively, by two kinds of modes, $\mu_2\text{-}\eta_2$ and $\mu_3\text{-}\eta_3\text{-}\eta_1$ modes with Ag–O distances of 2.399–2.874 Å (Fig. S2†).



Note that the $\{\text{SiW}_9\text{O}_{34}\}$ cluster has been used as a template to form the closed silver clusters because of its abundant terminal oxo atoms that can coordinate with the Ag^+ ions.³³ When the TMCC-substituted POMs formed by $\{\text{SiW}_9\text{O}_{34}\}$ and TM-coordination clusters are used as the templates, non-closed Ag_{38} clusters are formed, as found in **Ag₃₈-TM**. Obviously, the introduction of relatively large TM-coordination clusters can prevent the Ag^+ ions from wrapping around the entire TM_4SiW_9 template to form the closed silver clusters. It is also noteworthy that TM_4SiW_9 clusters have been reported for more than a decade,³⁴ but this is the first time that they have been recognized and introduced into the silver clusters as the templates for building the non-closed silver clusters.

To verify the validity of the synthesis concept and diversity of products, we carried out further exploration and successfully obtained two kinds of new non-closed silver clusters, **Ag₃₇-Zn** and **Ag₃₆-TM**. SCXRD analysis revealed that these compounds have the same TMCC-substituted POM template, $\{\text{TM}_5(\mu_3\text{-OH})_3(\text{Ac})_2(\text{SiW}_9\text{O}_{34})(\text{SiW}_{11}\text{O}_{39})\}$ (Fig. 3a), but slightly different non-closed silver shell structures. **Ag₃₇-Zn** also crystallizes in the $P\bar{1}$ space group and consists of a Zn_5 -substituted POM core of $\{\text{Zn}_5(\mu_3\text{-OH})_3(\text{Ac})_2(\text{SiW}_9\text{O}_{34})(\text{SiW}_{11}\text{O}_{39})\}$ ($\text{Zn}_5\text{Si}_2\text{W}_{20}$) and a 37-nuclearity non-closed silver shell of $\{\text{Ag}_{37}(\text{BuC}\equiv\text{C})_{22}(\text{NO}_3)_3\}$ (Ag_{37}). V-shaped $\text{Zn}_5\text{Si}_2\text{W}_{20}$ exhibits an unknown TMCC-substituted POM composed of a 5-nuclearity $\{\text{Zn}_5(\mu_3\text{-OH})_3(\text{Ac})_2\}$ zinc coordination cluster sandwiched by monolacunary $\{\text{SiW}_{11}\text{O}_{39}\}$ POM and trilacunary $\{\text{SiW}_9\text{O}_{34}\}$ POM (Fig. 3a). Alternatively, $\text{Zn}_5\text{Si}_2\text{W}_{20}$ can be viewed as a dimer consisting of Zn_4 -substituted Zn_4SiW_9 and a Keggin-type mono-Zn-substituted $\{\text{ZnSiW}_{11}\text{O}_{40}\}$ joined together by one edge-sharing

bioctahedral Zn_2O_{10} group and one corner-sharing bioctahedral ZnWO_{11} group, accompanied by the removal of one Ac^- ligand.

The skeleton of Ag_{37} in **Ag₃₇-Zn** can be derived from that of nest-like Ag_{38} in **Ag₃₈-Zn** by removing one Ag^+ ion from its upper Ag_{11} ring, wherein the vacancy after the removal of the Ag^+ ion is occupied by the fifth zinc ion from the $\text{Zn}_5\text{Si}_2\text{W}_{20}$ template (Fig. 3b and S3†). In addition, there is a difference between the peripheral ligands of Ag_{37} and Ag_{38} : that is, the CH_3CN ligand in Ag_{38} is replaced by a $\text{BuC}\equiv\text{C}^-$ ligand in Ag_{37} (Fig. S4†). Such a structural transformation suggests that silver cluster shells can respond simultaneously to changes in TMCC-substituted POM cores. The formation of **Ag₃₇-Zn** shows the tunability and flexibility of inner TMCC-substituted POM templates and further demonstrates the effectiveness of our synthetic strategy.

The manipulation of TM^{2+} ions with distinct electronic configurations presents a feasible method to fine-tune the structures and physicochemical properties of the products. In this regard, the use of cobalt and nickel salts led to the crystallization of **Ag₃₆-Co** and **Ag₃₆-Ni** (Fig. S5†). Energy dispersive spectroscopy elemental mapping spectra (Fig. S6–S12†) and crystal colors (Fig. S1†) confirmed the presence of different TM^{2+} ions in the clusters. **Ag₃₆-Co** and **Ag₃₆-Ni** have the same isomorphic TMCC-substituted POM template as **Ag₃₇-Zn**, but their silver shells differ slightly in the number of the Ag^+ ions and $\text{BuC}\equiv\text{C}^-$ ligands (Fig. S13 and S14†). The $\{\text{Ag}_{36}(\text{BuC}\equiv\text{C})_x\}$ (Ag_{36}) ($x = 18/17$ for Co/Ni) shells of **Ag₃₆-Co** and **Ag₃₆-Ni** can be derived from the further removal of one Ag^+ ion from the upper ZnAg_{10} ring of **Ag₃₇-Zn**, and the incorporated TM^{2+} ion is located near the fifth Zn^{2+} ion in **Ag₃₇-Zn** (Fig. S3†). Additionally, in response to the introduction of different TM^{2+} ions, the number of $\text{BuC}\equiv\text{C}^-$ ligands around the silver shell varied from 22 in **Ag₃₇-Zn** to 18 in **Ag₃₆-Co** and 17 in **Ag₃₆-Ni** (Fig. S14 and S15†). Results reveal that the TM^{2+} differences of the TMCC-substituted POM templates can precisely regulate Ag shells at the atomic level.

Notably, the obtainment of **Ag₃₇-Zn**, **Ag₃₆-Co** and **Ag₃₆-Ni** shows that the presence of TM clusters can not only cause the formation of broken silver clusters but also gather additional POM units (e.g. the monolacunary $\{\text{SiW}_{11}\text{O}_{39}\}$ POM in this work) to form unique non-closed structures with half the molecular template in the silver cluster and half outside the silver cluster. Interestingly, outside POM units have abundant terminal oxo atoms that can coordinate with the Ag^+ ions, which is expected to enable the non-closed silver clusters to undergo further assembly reactions. For example, by adjusting reaction parameters, an **Ag₃₇-Zn**-cluster-based two-dimensional (2D) infinitely extended structure $\{\text{Ag}_{37}\text{-Zn}\}_\infty$ was obtained. As shown in Fig. 4, the **Ag₃₇-Zn** cluster self-assembled into one-dimensional (1D) chains through the coordination of one terminal oxo atom of the outside $\{\text{SiW}_{11}\text{O}_{39}\}$ unit with one Ag^+ ion from the adjacent **Ag₃₇-Zn** cluster. Adjacent chains are further bridged into 2D layers by additional Ag^+ ions (with a site occupancy factor of 0.65), each of which forms a linear coordination with two oxo atoms from two $\{\text{SiW}_{11}\text{O}_{39}\}$ units (Fig. 4). Generally, closed alkynyl-protected silver clusters are difficult to assemble into extended structures due to the bulky steric hindrance of

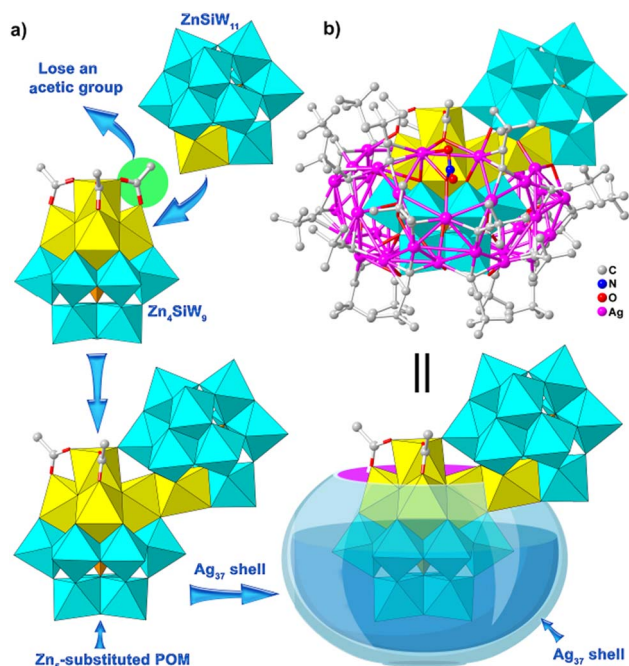


Fig. 3 (a) and (b) Views of the structures of the $\text{Zn}_5\text{Si}_2\text{W}_{20}$ template and **Ag₃₇-Zn**, respectively.

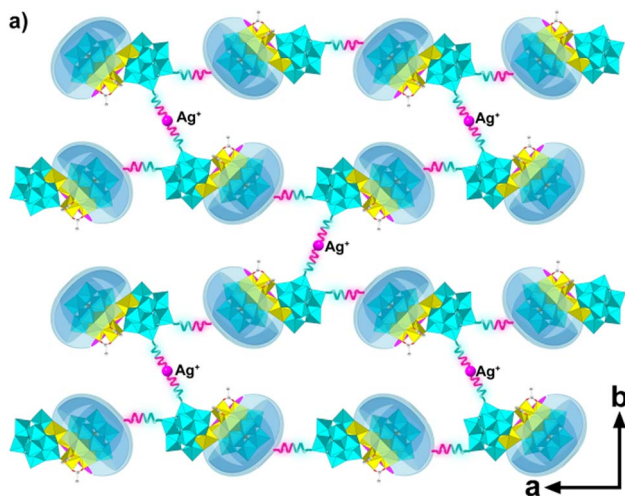


Fig. 4 Schematic diagram of the 2D structure $\{Ag_{37}\text{-Zn}\}_{\infty}$.

peripheral tertiary butyl groups.^{35–38} To date, only a few high-dimensional (2D/3D) structures have been reported, constructed from the silver clusters alone.^{39–43} $\{Ag_{37}\text{-Zn}\}_{\infty}$ represents a new 2D layer structure constructed with POM-templated silver cluster building blocks without auxiliary connecting ligands (Fig. S16†).^{44–46} Finally, the stacking of the 2D layers in $\{Ag_{37}\text{-Zn}\}_{\infty}$ produces irregular 1D channels of a size of about $4.18 \times 2.59 \text{ nm}^2$ along the *a* axis (Fig. S16b†), and the total potential solvent-accessible volume is $11\,658 \text{ \AA}^3$, occupying 38% of the volume of the unit cell. The acquisition of $\{Ag_{37}\text{-Zn}\}_{\infty}$ indicates that the synthetic strategy based on the TMCC-substituted POM templates also provides the possibility of the development of high-dimensional silver cluster-based framework materials. The successful syntheses of the various series of $Ag_{38}\text{-TM}$, $Ag_{37}\text{-TM}$ or $Ag_{36}\text{-TM}$ are attributed to the following synthetic strategy: using lacunary POMs to induce TMs and organic ligands to form TMCCs at their lacunary sites, thus forming the TMCC-substituted POMs for templating the formation of the non-closed silver clusters. Further, we find that non-closed silver cluster assembly reactions based on the above assembly strategy are sensitive to the reaction parameters; for example, different reaction times can form different products $Ag_{38}\text{-Zn}$ (1 day) and $Ag_{37}\text{-Zn}$ (3 days), and different starting silver reagents lead to different products $Ag_{37}\text{-Zn}$ and $Ag_{36}\text{-Co}$. These results indicate that the synthetic strategy is a feasible route to diversifying the structural family of the non-closed silver clusters.

It is worth mentioning at this point that Ozeki and co-workers reported two non-closed silver alkynyl clusters, $P_2W_{15}Nb_3@Ag_{25}$ and $(SiW_9Nb_3)_2@Ag_{42}$, using triniobium-oxo cluster-substituted POMs as the templates.^{16,17} In their synthetic method, the non-closed silver cluster was achieved by changing the affinity of the Ag^+ ions to the surface of the POM templates. They increased the surface negative charge of the top of the POM templates by the selective substitution of less positively charged Nb(v) for W(vi), leading to the preferential aggregation of the Ag^+ ions around triniobium-oxo clusters instead of tungsten-oxo clusters. In this work, the TMCC-

substituted POM templates in the four types of compounds also feature a non-uniform distribution of negative charges, but they have additional impacts on the formation of the series of the non-closed silver clusters. First, acetic ligands on the TMCC-substituted POM templates play a key role in preventing the Ag^+ ions from forming closed structures. Second, the POM templates with diverse TMCCs can enrich the structures of final non-closed silver clusters. Finally, the TMCC-substituted POM templates with unpaired electrons would introduce additional optical/electrical/magnetic properties into final composite clusters.

Due to the fascinating luminescent properties of the silver clusters,^{47–55} the luminescent characteristics of $Ag_{38}\text{-Zn}$, $Ag_{37}\text{-Zn}$ and $\{Ag_{37}\text{-Zn}\}_{\infty}$ were studied. $Ag_{38}\text{-Zn}$, $Ag_{37}\text{-Zn}$ and $\{Ag_{37}\text{-Zn}\}_{\infty}$ are all nearly emission-silent at room temperature. When the clusters are cooled gradually to low temperature, sharply enhanced emission can be observed in the near-infrared (NIR) region (Fig. 5a–c), which can be attributed to ligand-to-metal charge transfer (LMCT) or combination with metal-centered (MC) $d^{10} \rightarrow d^9 s^1$ transitions.⁵⁶ When cooled from 283 K to 83 K, $Ag_{38}\text{-Zn}$ exhibits wide-band emission, the maximum emission shifts from 696 to 708 nm, and the emission intensity increases by about 24 times, which can be assigned to the low-temperature-induced decrease in non-radiative decay.^{57,58} $Ag_{37}\text{-Zn}$ and $\{Ag_{37}\text{-Zn}\}_{\infty}$ exhibited similar emission spectra to

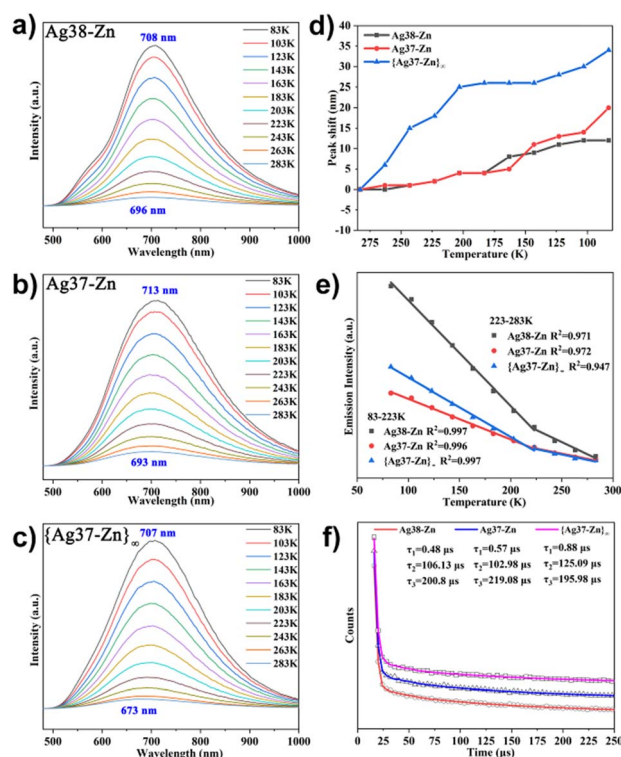


Fig. 5 (a)–(c) Temperature-dependent emission spectra of $Ag_{38}\text{-Zn}$, $Ag_{37}\text{-Zn}$ and $\{Ag_{37}\text{-Zn}\}_{\infty}$ in the range of 83–283 K, respectively. (d) Peak shift vs. temperature in the range of 83–283 K. (e) Plot of maximum emission intensity vs. temperature of three clusters fitted in the range of 83–223 and 223–283 K. (f) Emission decay curve of three clusters measured at 83 K.

Ag₃₈-Zn from 283 K to 83 K, except that the maximum emissions of **Ag₃₇-Zn** and **{Ag₃₇-Zn}_∞** shift from 693 nm to 713 nm and from 673 nm to 707 nm, respectively. The emission intensities of **Ag₃₇-Zn** and **{Ag₃₇-Zn}_∞** increase by about 14-fold and 22-fold as the temperature cools from 283 K to 83 K, respectively. In other words, the emission intensities of **Ag₃₈-Zn**, **Ag₃₇-Zn** and **{Ag₃₇-Zn}_∞** increase by 11.4%, 6.7% and 10.5% per K, respectively. The bathochromic shift may be due to reduced Ag⁺⋯Ag contacts at low temperature, which can decrease the energy gap of the MC transition to a certain extent. Interestingly, the degree of bathochromic shift of emission peaks is gradually enhanced from **Ag₃₈-Zn** (12 nm) to **Ag₃₇-Zn** (20 nm) to **{Ag₃₇-Zn}_∞** (34 nm), which may be caused by the increased bonding strength and enhanced rigidity of silver skeletons from **Ag₃₈-Zn** to **Ag₃₇-Zn** to **{Ag₃₇-Zn}_∞** (Fig. 5d).^{59,60} All the clusters showed good linear functions of emission intensity to temperature in the range of 223–83 K. The linear equation can be described as $I_{\max} = -8719T - 2240700$ with a correlation coefficient of 0.997 for **Ag₃₈-Zn**, $I_{\max} = -3355T - 891426$ with a correlation coefficient of 0.996 for **Ag₃₇-Zn**, and $I_{\max} = -4897T - 1220250$ with a correlation coefficient of 0.997 for **{Ag₃₇-Zn}_∞** (Fig. 5e). The good linearity suggests that **Ag₃₈-Zn**, **Ag₃₇-Zn** and **{Ag₃₇-Zn}_∞** may be potential sensors for luminescent thermometers to detect a broad range of temperature from 83 to 223 K. In fact, even in the temperature range of 283–223 K, the correlation coefficients of **Ag₃₈-Zn**, **Ag₃₇-Zn** and **{Ag₃₇-Zn}_∞** are 0.971, 0.972 and 0.947, respectively, also showing good linearity for the function of emission with temperature. All of their emission lifetimes fall into the microsecond scale at 83 K (Fig. 5f), indicating that their luminescences all display a triplet phosphorescence origin.^{61,62}

The introduction of the TM clusters can also endow the silver clusters with magnetic properties. The temperature-dependent magnetic susceptibilities of **Ag₃₈-Co** and **Ag₃₈-Ni** were measured in the temperature range of 2–300 K under an applied external field of 1 kOe (Fig. S17 and S18†). At 300 K, the $\chi_m T$ values of **Ag₃₈-Co** and **Ag₃₈-Ni** are 16.78 cm³ K mol^{−1} and 9.61 cm³ K mol^{−1}, respectively, which are lower than the theoretical values of 21.9 cm³ K mol^{−1} for four Co²⁺ ions ($g = 2$, $s = 3/2$) and 11.31 cm³ K mol^{−1} for four Ni²⁺ ions ($g = 2$ and $s = 1$). With cooling from 300 K to 2 K, the $\chi_m T$ values of **Ag₃₈-Co** and **Ag₃₈-Ni** decrease slowly at first in the range of 300–20 K and later rapidly decrease in the range of 20–2 K. The $\chi_m T$ values reach minimum values of 1.37 and 0.7 cm³ K mol^{−1} at 2 K, respectively. These behaviors indicate that **Ag₃₈-Co** and **Ag₃₈-Ni** are antiferromagnetic. These results are consistent with those of reported TM₄SiW₉ clusters,³⁴ suggesting that the antiferromagnetic properties of the TMCC cluster have been introduced to originally diamagnetic silver cluster materials.

Conclusions

In summary, we have successfully developed a synthetic method for constructing the rare non-closed silver clusters based on the TMCC-substituted POMs as the templates. With the method, four series of a total of seven new non-closed silver cluster species have been successfully synthesized, showing a fusion of

three distinct research areas of POM, TM clusters, and silver clusters. These examples provide atomically precise structural information on how the TMCC-substituted POM templates could prevent the Ag⁺ ions from forming closed clusters. Furthermore, the POM moiety and TMCC moiety of the TMCC-substituted POM templates show good tunability and flexibility, which provides the possibility for constructing diverse non-closed silver clusters. In particular, the TMCC moiety can further aggregate POMs, and it is expected to introduce giant high-nuclearity TMCC-substituted POMs into the assembly reaction of the silver clusters, which will show great potential in the construction of novel silver clusters, including high-dimensional cluster-based framework materials. Additionally, given their distinct physicochemical properties, the integration of TMCCs, POMs, and silver clusters into same molecular clusters is expected to endow the silver clusters with more abundant and unique optical, electrical, magnetic, and catalytic properties. The results demonstrate that the TMCC-substituted POM-templated synthetic strategy is a promising method for the development of unexplored non-closed multicomponent materials.

Data availability

The datasets supporting this article have been uploaded as part of the ESI.†

Author contributions

Rui Ge: investigation, data curation, writing – original draft; Ping-Wei Cai: characterization and methodology; Cai Sun: characterization and methodology; Yan-Qiong Sun: characterization and methodology; Xin-Xiong Li: writing – original draft, supervision, project administration, funding acquisition; Shou-Tian Zheng: supervision, project administration, funding acquisition.

Conflicts of interest

There are no conflicts to declare.

Acknowledgements

We gratefully acknowledge the financial support from the Natural Science Foundation of China (No. 92161108, 22171045, and 21971039), Natural Science Fund of Fujian Province (No. 2020J01438), and Key Program of Natural Science Foundation of Fujian Province (2021J02007).

References

- 1 Z. Wang, R. K. Gupta, G.-G. Luo and D. Sun, *Chem. Rec.*, 2020, **20**, 389–402.
- 2 W. Jing, H. Shen, R. Qin, Q. Wu, K. Liu and N. Zheng, *Chem. Rev.*, 2023, **123**, 5948–6002.
- 3 Y. Jin, C. Zhang, X.-Y. Dong, S.-Q. Zang and T. C. W. Mak, *Chem. Soc. Rev.*, 2021, **50**, 2297–2319.



- 4 X.-M. Luo, Y.-K. Li, X.-Y. Dong and S.-Q. Zang, *Chem. Soc. Rev.*, 2023, **52**, 383–444.
- 5 X. Kang and M. Zhu, *Coord. Chem. Rev.*, 2019, **394**, 1–38.
- 6 C. Sun, B. K. Teo, C. Deng, J. Lin, G.-G. Luo, C.-H. Tung and D. Sun, *Coord. Chem. Rev.*, 2021, **427**, 213576.
- 7 M.-M. Zhang, X.-Y. Dong, Y.-J. Wang, S.-Q. Zang and T. C. W. Mak, *Coord. Chem. Rev.*, 2022, **453**, 214315.
- 8 S.-S. Zhang, F. Alkan, H.-F. Su, C. M. Aikens, C.-H. Tung and D. Sun, *J. Am. Chem. Soc.*, 2019, **141**, 4460–4467.
- 9 Z. Wang, H.-F. Su, G.-L. Zhuang, M. Kurmoo, C.-H. Tung, D. Sun and L.-S. Zheng, *CCS Chem.*, 2019, **2**, 663–672.
- 10 S.-S. Zhang, S. Havenridge, C. Zhang, Z. Wang, L. Feng, Z.-Y. Gao, C. M. Aikens, C.-H. Tung and D. Sun, *J. Am. Chem. Soc.*, 2022, **144**, 18305–18314.
- 11 K.-G. Liu, X.-Y. Liu, Z.-J. Guan, K. Shi, Y.-M. Lin and Q.-M. Wang, *Chem. Commun.*, 2016, **52**, 3801–3804.
- 12 X. Fan, S. Chen, L. Zhang and J. Zhang, *Chem.–Eur. J.*, 2021, **27**, 15563–15570.
- 13 K. Yonesato, H. Ito, D. Yokogawa, K. Yamaguchi and K. Suzuki, *Angew. Chem., Int. Ed.*, 2020, **59**, 16361–16365.
- 14 Z. Wang, L. Li, L. Feng, Z.-Y. Gao, C.-H. Tung, L.-S. Zheng and D. Sun, *Angew. Chem., Int. Ed.*, 2022, **61**, e202200823.
- 15 Z. Wang, H.-F. Su, L.-P. Zhang, J.-M. Dou, C.-H. Tung, D. Sun and L. Zheng, *ACS Nano*, 2022, **16**, 4500–4507.
- 16 M. Kurasawa, F. Arisaka and T. Ozeki, *Inorg. Chem.*, 2015, **54**, 1650–1654.
- 17 S. Tamari, K. Ono, M. Hashimoto and T. Ozeki, *Dalton Trans.*, 2015, **44**, 19056–19058.
- 18 S.-S. Zhang, J.-Y. Chen, K. Li, J.-D. Yuan, H.-F. Su, Z. Wang, M. Kurmoo, Y.-Z. Li, Z.-Y. Gao, C.-H. Tung, D. Sun and L. Zheng, *Chem. Mater.*, 2021, **33**, 9708–9714.
- 19 F. Gruber and M. Jansen, *Angew. Chem., Int. Ed.*, 2010, **49**, 4924–4926.
- 20 X. Kang and M. Zhu, *ACS Cent. Sci.*, 2022, **8**, 1235–1237.
- 21 Y. Li, Q.-X. Zang, X.-Y. Dong, Z.-Y. Wang, P. Luo, X.-M. Luo and S.-Q. Zang, *ACS Cent. Sci.*, 2022, **8**, 1258–1264.
- 22 F. Hu, R.-L. He, Z.-J. Guan, C.-Y. Liu and Q.-M. Wang, *Angew. Chem., Int. Ed.*, 2023, **62**, e202304134.
- 23 F. Hu, H.-W. Luyang, R.-L. He, Z.-J. Guan, S.-F. Yuan and Q.-M. Wang, *J. Am. Chem. Soc.*, 2022, **144**, 19365–19371.
- 24 Y. Li, X.-M. Luo, P. Luo, Q.-X. Zang, Z.-Y. Wang and S.-Q. Zang, *ACS Nano*, 2023, **17**, 5834–5841.
- 25 X.-M. Luo, S. Huang, P. Luo, K. Ma, Z.-Y. Wang, X.-Y. Dong and S.-Q. Zang, *Chem. Sci.*, 2022, **13**, 11110–11118.
- 26 Q. Chang, X. Meng, W. Ruan, Y. Feng, R. Li, J. Zhu, Y. Ding, H. Lv, W. Wang, G. Chen and X. Fang, *Angew. Chem., Int. Ed.*, 2022, **61**, e202117637.
- 27 Q.-S. Lai, X.-X. Li and S.-T. Zheng, *Coord. Chem. Rev.*, 2023, **482**, 215077.
- 28 J. Liu, M. Huang, X. Zhang, Z. Hua, Z. Feng, Y. Dong, T. Sun, X. Sun and C. Chen, *Coord. Chem. Rev.*, 2022, **472**, 214785.
- 29 J.-C. Liu, J.-W. Zhao, C. Streb and Y.-F. Song, *Coord. Chem. Rev.*, 2022, **471**, 214734.
- 30 N. Ogiwara, T. Iwano, T. Ito and S. Uchida, *Coord. Chem. Rev.*, 2022, **462**, 214524.
- 31 Z. Zeb, Y. Huang, L. Chen, W. Zhou, M. Liao, Y. Jiang, H. Li, L. Wang, L. Wang, H. Wang, T. Wei, D. Zang, Z. Fan and Y. Wei, *Coord. Chem. Rev.*, 2023, **482**, 215058.
- 32 K. Yonesato, D. Yanai, S. Yamazoe, D. Yokogawa, T. Kikuchi, K. Yamaguchi and K. Suzuki, *Nat. Chem.*, 2023, **15**, 940–947.
- 33 G.-X. Duan, Y.-P. Xie, J.-L. Jin, L.-P. Bao, X. Lu and T. C. W. Mak, *Chem.–Eur. J.*, 2018, **24**, 6762–6768.
- 34 C. Pichon, P. Mialane, A. Dolbecq, J. Marrot, E. Rivière, B. S. Bassil, U. Kortz, B. Keita, L. Nadjo and F. Sécheresse, *Inorg. Chem.*, 2008, **47**, 11120–11128.
- 35 F. Hu, J.-J. Li, Z.-J. Guan, S.-F. Yuan and Q.-M. Wang, *Angew. Chem., Int. Ed.*, 2020, **59**, 5312–5315.
- 36 W.-D. Liu, J.-Q. Wang, S.-F. Yuan, X. Chen and Q.-M. Wang, *Angew. Chem., Int. Ed.*, 2021, **60**, 11430–11435.
- 37 M. Zhao, S. Huang, Q. Fu, W. Li, R. Guo, Q. Yao, F. Wang, P. Cui, C.-H. Tung and D. Sun, *Angew. Chem., Int. Ed.*, 2020, **59**, 20031–20036.
- 38 S.-F. Yuan, Z.-J. Guan and Q.-M. Wang, *J. Am. Chem. Soc.*, 2022, **144**, 11405–11412.
- 39 K. Zhou, C. Qin, H.-B. Li, L.-K. Yan, X.-L. Wang, G.-G. Shan, Z.-M. Su, C. Xu and X.-L. Wang, *Chem. Commun.*, 2012, **48**, 5844–5846.
- 40 G. Deng, B. K. Teo and N. Zheng, *J. Am. Chem. Soc.*, 2021, **143**, 10214–10220.
- 41 C. Wang, Y.-J. Wang, C.-L. He, Q.-Y. Wang and S.-Q. Zang, *JACS Au*, 2021, **1**, 2202–2207.
- 42 C.-H. Gong, Z.-B. Sun, M. Cao, X.-M. Luo, J. Wu, Q.-Y. Wang, S.-Q. Zang and T. C. W. Mak, *Chem. Commun.*, 2022, **58**, 9806–9809.
- 43 X. Jing, F. Fu, R. Wang, X. Xin, L. Qin, H. Lv and G.-Y. Yang, *ACS Nano*, 2022, **16**, 15188–15196.
- 44 Z. Wang, Y.-J. Zhu, Y.-Z. Li, G.-L. Zhuang, K.-P. Song, Z.-Y. Gao, J.-M. Dou, M. Kurmoo, C.-H. Tung and D. Sun, *Nat. Commun.*, 2022, **13**, 1802.
- 45 Z. Wang, Y.-M. Sun, Q.-P. Qu, Y.-X. Liang, X.-P. Wang, Q.-Y. Liu, M. Kurmoo, H.-F. Su, C.-H. Tung and D. Sun, *Nanoscale*, 2019, **11**, 10927–10931.
- 46 K. Sheng, Z. Wang, L. Li, Z.-Y. Gao, C.-H. Tung and D. Sun, *J. Am. Chem. Soc.*, 2023, **145**, 10595–10603.
- 47 P. Sun, Z. Wang, Y. Bi, D. Sun, T. Zhao, F. Zhao, W. Wang and X. Xin, *ACS Appl. Nano Mater.*, 2020, **3**, 2038–2046.
- 48 W.-M. He, Z. Zhou, Z. Han, S. Li, Z. Zhou, L.-F. Ma and S.-Q. Zang, *Angew. Chem., Int. Ed.*, 2021, **60**, 8505–8509.
- 49 Z.-R. Yuan, Z. Wang, B.-L. Han, C.-K. Zhang, S.-S. Zhang, Z.-Y. Zhu, J.-H. Yu, T.-D. Li, Y.-Z. Li, C.-H. Tung and D. Sun, *Angew. Chem., Int. Ed.*, 2022, **134**, e202211628.
- 50 X. Kang, Y. Li, M. Zhu and R. Jin, *Chem. Soc. Rev.*, 2020, **49**, 6443–6514.
- 51 J. Dou, B. Chen, G. Liu, X. Dong, W. Yu, J. Wang, Y. Zhang, Z. Li and J. Zhu, *J. Rare Earths*, 2022, **40**, 193–200.
- 52 J. Hong, L. Lin, X. Li, Z. Feng, L. Huang, Q. Qin and Z. Zheng, *J. Rare Earths*, 2020, **38**, 1151–1157.
- 53 M.-M. Zhang, X.-Y. Dong, Z.-Y. Wang, X.-M. Luo, J.-H. Huang, S.-Q. Zang and T. C. W. Mak, *J. Am. Chem. Soc.*, 2021, **143**, 6048–6053.
- 54 Z. Han, X.-Y. Dong, P. Luo, S. Li, Z.-Y. Wang, S.-Q. Zang and T. C. W. Mak, *Sci. Adv.*, 2020, **6**, eaay0107.



- 55 S.-S. Zhang, R.-C. Liu, X.-C. Zhang, L. Feng, Q.-W. Xue, Z.-Y. Gao, C.-H. Tung and D. Sun, *Sci. China: Chem.*, 2021, **64**, 2118–2124.
- 56 V. W.-W. Yam, V. K.-M. Au and S. Y.-L. Leung, *Chem. Rev.*, 2015, **115**, 7589–7728.
- 57 Y.-M. Su, W. Liu, Z. Wang, S.-A. Wang, Y.-A. Li, F. Yu, Q.-Q. Zhao, X.-P. Wang, C.-H. Tung and D. Sun, *Chem.–Eur. J.*, 2018, **24**, 4967–4972.
- 58 Y.-M. Su, Z.-Z. Cao, L. Feng, Q.-W. Xue, C.-H. Tung, Z.-Y. Gao and D. Sun, *Small*, 2022, **18**, 2104524.
- 59 B. Li, R.-W. Huang, J.-H. Qin, S.-Q. Zang, G.-G. Gao, H.-W. Hou and T. C. W. Mak, *Chem.–Eur. J.*, 2014, **20**, 12416–12420.
- 60 Y. Zhou, L. Liao, S. Zhuang, Y. Zhao, Z. Gan, W. Gu, J. Li, H. Deng, N. Xia and Z. Wu, *Angew. Chem., Int. Ed.*, 2021, **60**, 8668–8672.
- 61 R.-W. Huang, Y.-S. Wei, X.-Y. Dong, X.-H. Wu, C.-X. Du, S.-Q. Zang and T. C. W. Mak, *Nat. Chem.*, 2017, **9**, 689–697.
- 62 Z.-Y. Wang, M.-Q. Wang, Y.-L. Li, P. Luo, T.-T. Jia, R.-W. Huang, S.-Q. Zang and T. C. W. Mak, *J. Am. Chem. Soc.*, 2018, **140**, 1069–1076.

